A Reliable Method for the Extraction of the Lateral Position of Defects in Ultra-scaled MOSFETs

Yu.Yu. Illarionov*†, M. Bina*, S.E. Tyaginov*†, K. Rott‡, H. Reisinger‡, B. Kaczer§ and T. Grasser*

* Institute for Microelectronics, TU Wien, Austria
† Ioffe Physical-Technical Institute, Russia
‡ Infineon, Munich, Germany
§ imec, Leuven, Belgium

***Abstract*—We propose a new method to determine the lateral position of border traps in MOSFETs. The approach is based on the dependence of the trap-induced threshold voltage shift on the drain bias which is sensitive to the trap position. This follows from the results obtained with both technology computer aided design (TCAD) simulations and with a compact model. Using our novel method we extract the lateral position of a number of experimentally observed traps. We show that even in the presence of random dopants the lateral position of the trap can be determined with a precision of several nanometers. Considering random dopants is one of the key features of our method. The compact model essentially allows to avoid time consuming TCAD simulations without significant loss of accuracy.**

I. Introduction

The impact of interface and oxide traps on MOSFET characteristics is crucial and still of fundamental importance [1–11]. Modern nanoscale MOSFETs contain merely a handful of defects [7] which can heavily disturb the device electrostatics. Charging and discharging of these defects leads to a time-dependent variability of the transistor characteristics, which eventually determines the lifetime of the device [5, 9]. As a consequence, the device reliability has to be studied from a statistical point of view, and thus much information about defect energetical properties [5, 6] and the depth position in the oxide film [3] has been obtained recently. However, there is no reliable method which can reveal the lateral trap position. This information is of great importance because charged defects situated in different sections of the device can have a substantionally different impact on the performance. In particular, experiments show that the magnitude of the threshold voltage shift and its dependence on the drain bias may be fundamentally different for the long defect (Fig. 1). So far, only a few attempts to extract the lateral trap position have been undertaken [3, 4, 12]. In the most recent technique [12], a relation between the position of the channel barrier peak and the random telegraph noise (RTN) magnitude is employed. However, the significant impact of the traps and the random dopants on the shape of the potential profile has not been properly addressed (Fig. 2), which may lead to unpredictable results on the lateral trap position evaluation. Another method proposed in Ref. [3] is also based on the RTN analysis but focuses mainly on the vertical depth rather than the lateral position. Therefore, a method which can extract the trap lateral coordinate in the presence of random dopants is urgently needed. We present a new approach which exploits the correlation between the drain bias dependence of the threshold voltage shift ΔV_{th} and the defect position X_T. The method considers the effect of random dopants, which leads to some uncertainty in the extracted trap position. Finally, the accuracy of the method is discussed using experimental data.

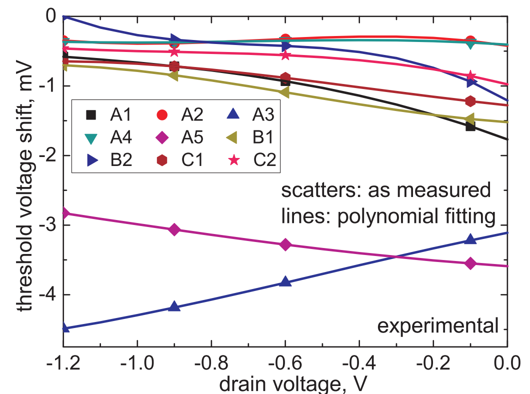

Fig. 1: Experimentally measured $\Delta V_{th}(V_d)$ characteristics of 9 individual traps. All the results are perfectly fitted with a cubic polynomial function: $\Delta V_{th}(V_d)=p_3 V_d{}^3+p_2 V_d^2+p_1 V_d+p_0$. As will be shown, the unique set of fitting coefficients p_i can be used to determine the lateral trap position X_T.

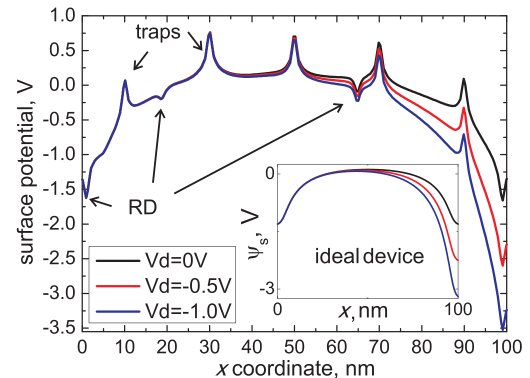

Fig. 2: Surface potential distribution along the interface of the test device with five traps and random dopants(RD). The potential distribution for an ideal device (i.e. without traps and random dopants) is given in the inset. Source corresponds to x=0 nm and Drain to x=100 nm.

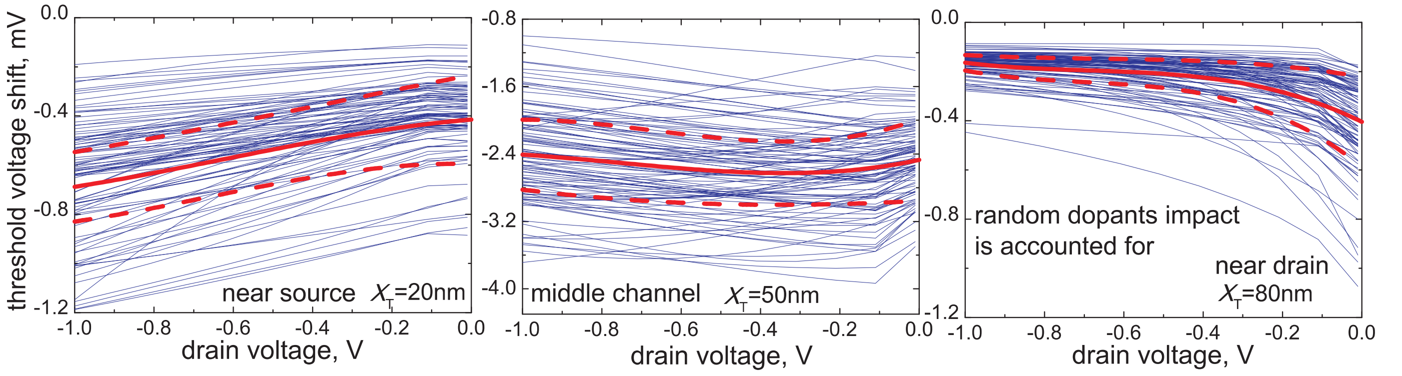

Fig. 3: TCAD simulated $\Delta V_{th}(V_d)$ characteristics for devices with different random dopant configurations and a fixed trap position X_T. **Left**: The trap is situated at the source side of the channel; **Center:** in the middle of the channel, and **Right**: at the drain side of the channel. The red lines indicate the characteristics with average (solid) and plus/minus standard deviation polynomial coefficients (dashed). The shape of the $\Delta V_{th}(V_d)$ curves depends on the trap position much stronger than on the random dopant distribution, and thus can be used as a fingerprint.

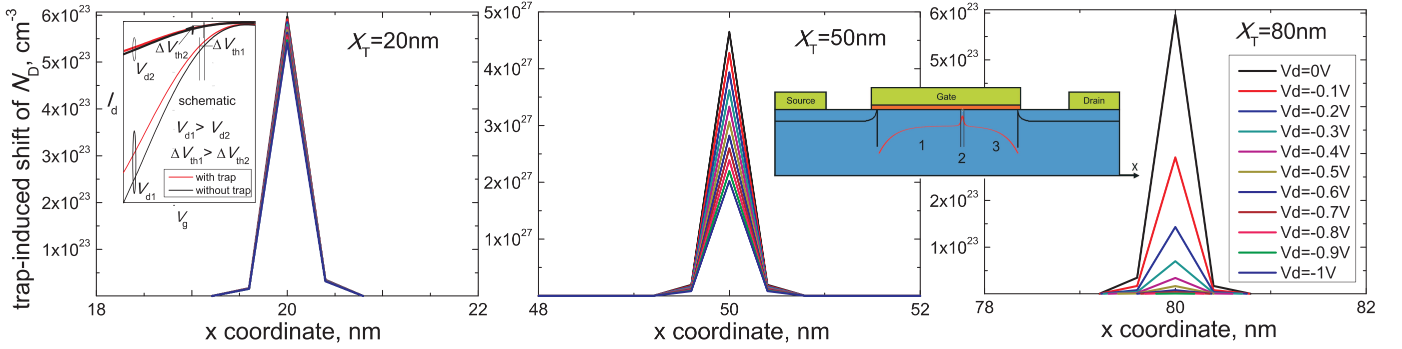

Fig. 4: The presence of trap-induced spikes (e.g. Fig. 2) can be treated as an artificial δ-like local increase of N_D. Its magnitude can be calculated for any X_T if the surface potential distribution is known (note different y scales). **Left**: A weak V_d dependence at the source side leads to the main impact of I_d-V_g vs. V_d (inset) on $\Delta V_{th}(V_d)$, leading to $\Delta V_{th}(V_d)$ going up. **Center:** Higher peak in the middle of the channel leads to a bigger ΔV_{th}. **Right**: A strong decrease of the peak height vs. V_d at the drain side leads to $\Delta V_{th}(V_d)$ going down. These dependences are introduced in the simulations based on the Enz-Krummenacher-Vittoz (EKV) model which allows to obtain the I_d-V_g characteristics.

II. Experiment

Oxide defects in p-MOSFETs with 2.2 nm SiON oxide films and W/L = 150 nm/100 nm were repeatedly charged and discharged using the time-dependent defect spectroscopy [13–15]. As each device contains only a handful of defects, the threshold voltage shift ΔV_{th} induced by each trap can be traced individually versus the drain bias V_d. The results obtained in three different devices are shown in Fig. 1. Quite clearly, the measured $\Delta V_{th}(V_d)$ dependences are dramatically different, indicating that the traps are located in different regions of the device [4]. Based on this, we parameterize the $\Delta V_{th}(V_d)$ dependences and approximate them by a cubic function of V_d. As will be shown, the corresponding coefficients are unique for each particular trap position. Therefore, this *unique set of coefficients* can be treated as *the defect signature* and used for precise identification of the trap position.

III. TCAD simulations

We performed TCAD simulations employing the density gradient method [16] for a hundred devices with identical architecture but with different distributions of random dopants. For each device we calculated two I_d-V_g curves, one with and one without a single trap. In order to provide a benchmark for the extraction algorithm, the lateral trap position along the oxide/Si interface (X_T) was varied from the source to the drain in 10 nm steps. The trap position in the direction perpendicular to the source-channel-drain plane was set to be W_T = 0.5 W as this was found not to have any essential impact on the shape of $\Delta V_{th}(V_d)$ curves. The trap induced ΔV_{th} as a function of V_d were extracted for a fixed $V_g \leq V_{th}$ (i.e. weak inversion mode) from the analysis of the I_d-V_g curves simulated for the devices with charged and uncharged traps.

The obtained $\Delta V_{th}(V_d)$ characteristics show a cubic behavior, just as their experimental counterparts. In Fig. 3 one can see the examples of $\Delta V_{th}(V_d)$ characteristics extracted from the results of TCAD simulations for three different trap positions. It is clearly seen that the shape of these curves is strongly dependent on the lateral defect position X_T. For example, if the trap is situated at the source side of the channel, the threshold voltage shift ΔV_{th} increases versus the drain bias V_d (Fig. 3, left). For the trap in the middle of the device the dependence of ΔV_{th} on V_d is rather weak (Fig. 3, center), while for the trap situated at the drain side ΔV_{th} decreases with V_d (Fig. 3, right). It is also clear that the impact of the lateral trap position X_T on the shape of $\Delta V_{th}(V_d)$ characteristics is much stronger than the impact of random dopants distribution. This is the key statement which introduces the concept of the trap location technique based on the correlation between the shape of the

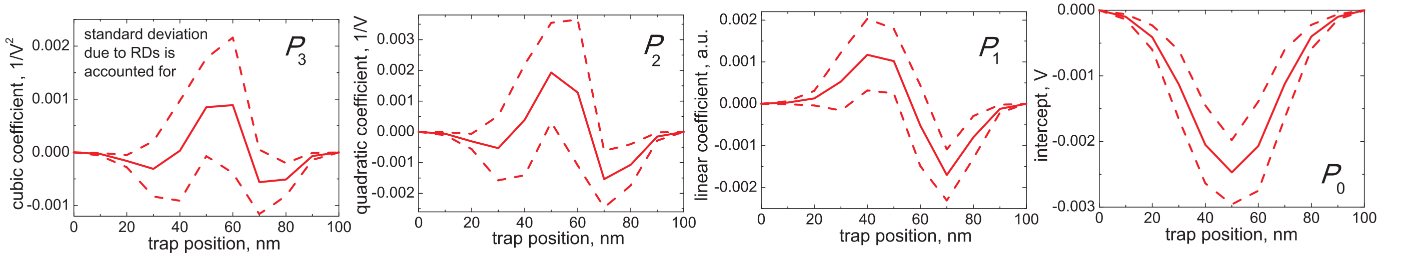

Fig. 5: The dependences of the parameterization coefficients of the $\Delta V_{\mathrm{th}}(V_{\mathrm{d}})$ characteristics on X_{T} simulated with TCAD showing the different behavior of the $\Delta V_{\mathrm{th}}(V_{\mathrm{d}})$ curves. For example, the slope changes sign near the middle of the channel. The highest absolute values of P_0 are also reached near the middle of the channel, and thus the maximum ΔV_{th} is reached there (cf. Refs. [4, 17]).

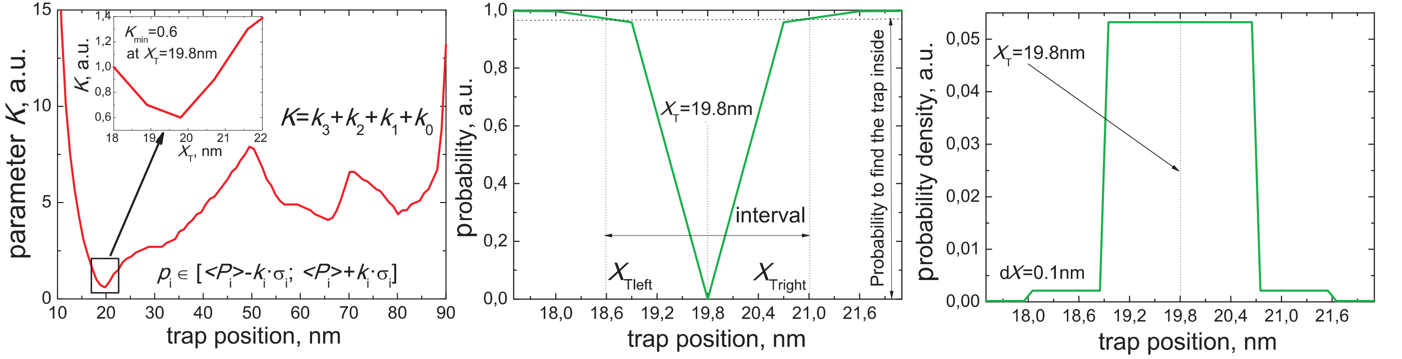

Fig. 6: Illustration of the working principle of our method for $X_{\mathrm{T}}=20\,\mathrm{nm}$. **Left**: A typical K vs. X_{T} dependence. K determines the proximity of the experimental $\Delta V_{\mathrm{th}}(V_{\mathrm{d}})$ to the mean TCAD curve. K_{min} is observed at X_{T}=19.8 nm. **Center:** The probability to find the trap inside several intervals around an extracted X_{T}. This is equal to the probability with which the points $X_{\mathrm{T_{left}}}$, X_{T} and $X_{\mathrm{T_{right}}}$ can be separated with respect to the narrowest intervals $[\langle P_i\rangle$-$k_i\sigma_i$; $\langle P_i\rangle$+$k_i\sigma_i]$ selected at each position. **Right**: The probability density corresponding to the interval dX=0.1 nm. The origin of such a distribution is random dopant effects.

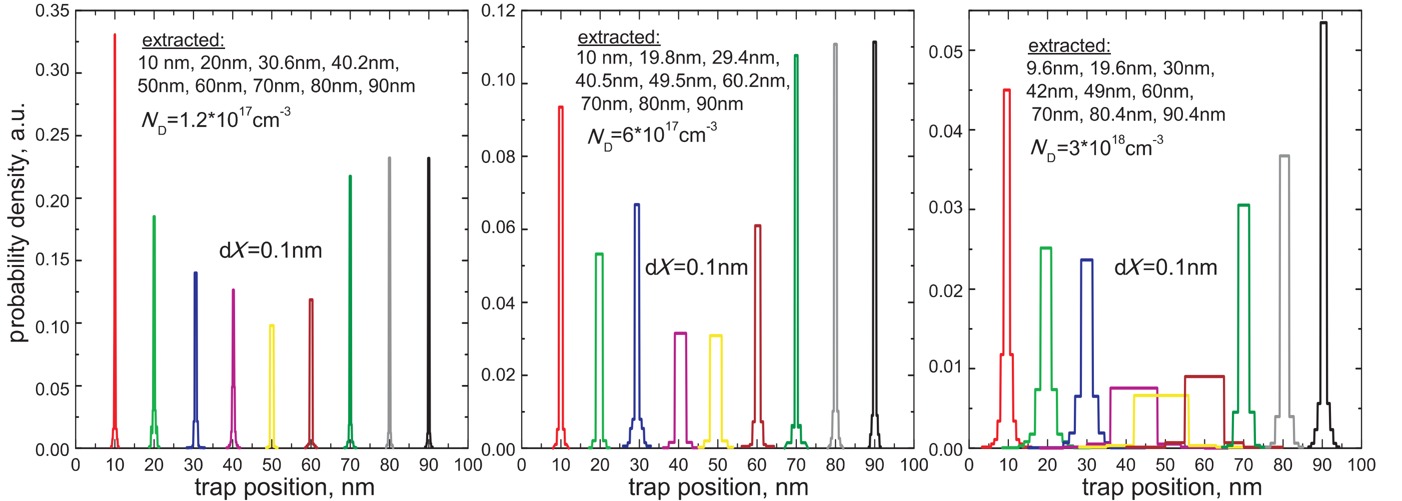

Fig. 7: The probability densities obtained for similar devices with three different doping concentrations. The simulated X_{T} is varied between 10 nm and 90 nm in 10 nm steps. The $\Delta V_{\mathrm{th}}(V_{\mathrm{d}})$ characteristic is selected to be closest to the average TCAD curve in order to find the best accuracy which can be achieved with the method. In all cases the impact of random dopants is stronger in the middle of the channel. The best accuracy is reached for the device with the lowest N_{D}.

$\Delta V_{\mathrm{th}}(V_{\mathrm{d}})$ characteristics and the lateral trap position.

IV. Compact model

As the TCAD simulations are extremely time consuming, we attempt to capture the essence in an analytical manner. We describe the border trap impact on the device performance in terms of channel doping level fluctuations by assuming that the trap-induced increase of majority carrier concentration (electrons in the case of p-MOSFET) is equivalent to a local abrupt increase of the channel doping level N_{D}. This feature is directly related to the trap-induced surface potential perturbations, because the carrier concentration is an exponential function of the surface potential. For example, the electron concentration shift induced by the border trap at $V_{\mathrm{d}}=0$ is given as

$$\Delta \mathrm{N_e}(x) = N_{\mathrm{D}}\left(\mathrm{e}^{\frac{\psi_{\mathrm{s}}^{0}(x)+\psi_{\mathrm{s}}^{T0}(x)}{kT}} - \mathrm{e}^{\frac{\psi_{\mathrm{s}}^{0}(x)}{kT}}\right) \tag{1}$$

Here $\psi_s^0(x){=}\psi_s(x{,}V_d{=}0)$ is the surface potential along the interface for the uncharged structure and $\psi_s^{T0}(x){=}\psi_s^T(x{,}V_d{=}0)$ is a peak function centered at $x{=}X_T$ which describes the local shift of $\psi_s^0(x)$ in the charged structure, i.e. the trap-induced spike similar to the results given in Fig. 2. The quantity $\psi_s^{T0}(x)$ is universal for each device and can be accurately fitted using a Voigt-like peak function as

$$\psi_s^{T0}(x) = \pm \frac{V_0}{1+\left(\frac{x-X_T}{x_0}\right)^2} \quad (2)$$

The plus sign has to be taken for an p-MOSFET and minus for an n-MOSFET, the scaling factor V_0 determines the spike height and is independent on X_T (for most of the N_D values typical for MOSFETs V_0 lies within the range 0.4...1 V) and $x_0{=}1\,\text{nm}$. The surface potential in uncharged structure $\psi_s^0(x)$ is obtained using an analytical model [18] which we have adjusted for the case of a deep junction. Then the channel is divided into three regions (Fig. 4, right inset) similarly to Refs. [19, 20]. The two regions 1 and 3 in which $\psi_s^{T0}(x) \ll \psi_s^{T0}(x{=}X_T)$ are assumed to be unperturbed. The region 2 with essential trap-induced perturbation $\psi_s^{T0}(x)$ is considered to be perturbed. Thus, we assume that the donor concentration inside the unperturbed regions is constant versus the coordinate and equal to the nominal N_D. Inside the perturbed region the quantity ΔN_D which is equivalent to the trap-induced carrier concentration shift ΔN_e has to be added to N_D. Considering the drain bias dependence the equation (1) can be rewritten as

$$\Delta \mathrm{N_D}(x) = N_D\left(\mathrm{e}^{\frac{\psi_s^0(x)+\psi_s^{T0}(x)+\delta\psi_s^T(X_T,V_d)}{kT}} - \mathrm{e}^{\frac{\psi_s^0(x,V_d)}{kT}}\right) \quad (3)$$

Here the dependence $\psi_s^0(x{,}V_d)$ is described by the model given in Ref. [18] and $\delta\psi_s^T(X_T{,}V_d)$ is the V_d-induced surface potential shift introduced in our model [20]. In Ref. [20] it has been demonstrated that the V_d dependence of the surface potential inside the perturbed region strongly correlates with the lateral trap position.

Thus, the height and the V_d dependences of the obtained ΔN_D peaks are strongly linked to the trap position, as one can see in Fig. 4. For example, the impact of the traps situated in the middle of the channel is equivalent to a much higher doping level shift than it would be for traps situated near the electrodes. This explains the higher values ΔV_{th} in such a case (e.g. Fig. 3). Also, the behavior of $\delta\psi_s^T(X_T{,}V_d)$ analyzed in Ref. [20] leads to a weak V_d dependence of the peak height for the traps situated at the source side of the channel. This means that the $\Delta V_{th}(V_d)$ dependence in such a case is completely determined by I_d-V_g versus V_d behavior (Fig. 4, left inset). In other words, for small V_d the values of ΔV_{th} are smaller, and thus the slope of the $\Delta V_{th}(V_d)$ is positive. Conversely, the traps situated at the drain side of the channel induce a doping level shift which is strongly dependent on V_d. Hence, the peaks are essentially smaller for higher V_d. This leads to a higher ΔV_{th} for small values of the drain bias, leading to a negative slope of the $\Delta V_{th}(V_d)$ curves. If the trap is situated in the middle of the channel, the two mentioned effects have a comparable magnitude and nearly compensate each other, leading to a weak $\Delta V_{th}(V_d)$ dependences.

Based on these observations we implemented the obtained doping level profiles into the Enz-Krummenacher-Vittoz (EKV) model [21] and simulated the I_d-V_g characteristics for devices with a single trap as well as for the devices without traps, where a constant N_D has been used. Similarly to the TCAD simulations, the trap induced ΔV_{th} was extracted from I_d-V_g curves as a function of V_d. The random potential perturbations due to random dopants were also incorporated into the surface potential in order to describe the random dopant effects.

V. Method description

We proceed first by fitting the TCAD data with $\Delta V_{th}(V_d){=}P_3V_d{}^3{+}P_2V_d^2{+}P_1V_d{+}P_0$, where the coefficients P_i are functions of the determined trap position X_T. By matching these polynomials to their experimental counterparts the lateral trap position can be extracted. This is done according to an algorithm which compares the qubic parameterization coefficients p_i obtained from the experimental data (e.g., Fig. 1) with those P_i simulated by TCAD. Their dependences on the lateral trap position are represented in Fig. 5. The principle of this method is illustrated in Fig. 6. For each X_T one can find such a minimal k_i guaranteeing that p_i lie inside the intervals $[\langle P_i\rangle\text{-}k_i\sigma_i;\ \langle P_i\rangle{+}k_i\sigma_i]$. Here $\langle P_i\rangle$ are the mean TCAD coefficients and σ_i the standard deviations due to random dopants (Fig. 3). The sum $K{=}k_3{+}k_2{+}k_1{+}k_0$ defines the proximity between experimental and TCAD data. Thus, the value of X_T at which the combination of p_i lies closest to the corresponding $\langle P_i\rangle$, i.e. the parameter K reaches its minimal value (Fig. 6, left), is considered as the extracted lateral trap position X_T.

After this the probability that all four intervals $[\langle P_i\rangle\text{-}k_i\sigma_i;\ \langle P_i\rangle{+}k_i\sigma_i]$ obtained for an extracted X_T do not intersect simultaneously with similar intervals for neighboring points X_{Tleft} and X_{Tright} can be found. This is then interpreted as the probability of finding the trap inside the interval $[X_{Tleft}, X_{Tright}]$ centered at the extracted X_T (Fig. 6, center). Its distribution can be replotted in terms of a normalized density (Fig. 6, right), which is obtained for each X_T and dX as a probability to find the trap inside the fixed interval $[X_T\text{-d}X; X_T\text{+d}X]$. Note that the consideration of all four coefficients results in a high accuracy of the lateral trap position evluation.

VI. Method verification

We check if the reverse algorithm reproduces the benchmark X_T. For this purpose we chose one of the $\Delta V_{th}(V_d)$ curves (which is closest to the mean curve) obtained for a certain doping configuration. Then this curve is used to play the role of the experimental data and the method is applied to these data in order to estimate the optimum accuracy. The obtained probability densities calculated for different N_D are plotted in Fig. 7. In all cases the uncertainty in determined X_T rarely exceeds 2 nm. Interestingly, the distributions are broader near the middle of the channel, which is due to a stronger impact of random dopants [17] on the device electrostatics and also due to a weak $\Delta V_{th}(V_d)$ dependence (e.g., Fig. 3, center). Another important feature is that the accuracy substantially decreases with increasing doping level. The origin of this is also due

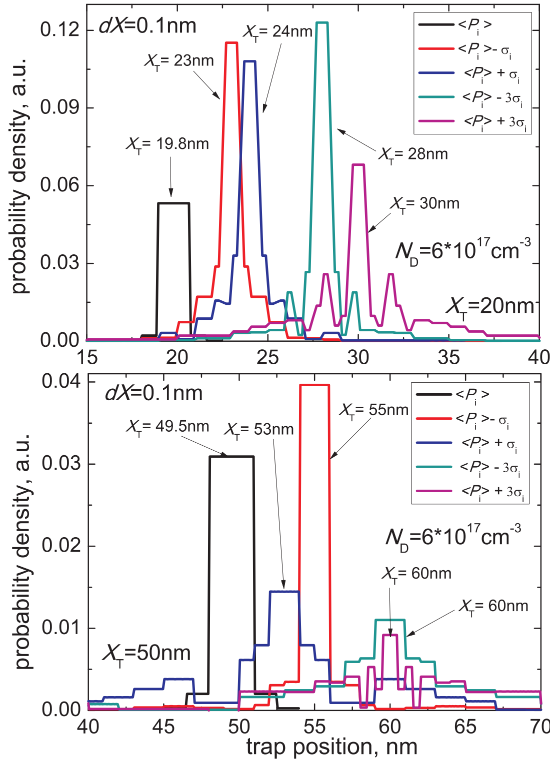

Fig. 8: The probability densities obtained for devices with the same doping level N_{D} but with a different deviation of random dopant configurations from the mean. **Top**: The border trap is situated at $X_{\mathrm{T}}=20\,\mathrm{nm}$. **Bottom**: The defect position is $X_{\mathrm{T}}=50\,\mathrm{nm}$. The X_{T} value extracted for an ideal case ($P_i=\langle P_i\rangle$) is nearly the same as the real trap position. For a case of stronger random dopant impact ($P_i=\langle P_i\rangle\pm\sigma_i$) the error is around 3-5 nm, and for extremely strong deviations of random dopant configurations from the mean ($P_i=\langle P_i\rangle\pm3\sigma_i$) it is around 8-10 nm.

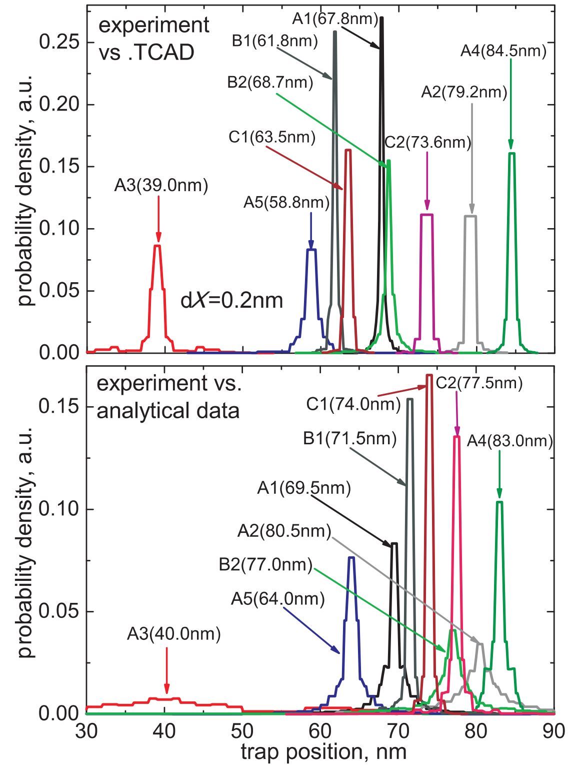

Fig. 9: The trap positions extracted from the experimental data. The results are plotted in terms of the probability densities calculated for the small intervals $dX=0.2\,\mathrm{nm}$. **Top**: The results obtained using TCAD data. **Bottom**: The compact model data results. The deviation of the extracted X_{T} is typically $\leq 10\,\mathrm{nm}$.

to the weak $\Delta V_{\mathrm{th}}(V_{\mathrm{d}})$ dependence observed for the devices with high N_{D}. This makes the impact of random dopants more pronounced.

As a further verification step we have applied our algorithm to the characteristics obtained for the devices with configurations of random dopants different from the mean, for which $\Delta V_{\mathrm{th}}(V_{\mathrm{d}})$ curves are situated farther from the mean curve, i.e. the deviation of the parameterization coefficients from $\langle P_i\rangle$ is stronger. The obtained results plotted in terms of the normalized probability density are represented in Fig. 8. They correspond to devices with the border trap situated at $X_{\mathrm{T}}=20\,\mathrm{nm}$ and at $X_{\mathrm{T}}=50\,\mathrm{nm}$. The $\Delta V_{\mathrm{th}}(V_{\mathrm{d}})$ characteristics with $P_i=\langle P_i\rangle\pm\sigma_i$ and $\langle P_i\rangle\pm3\sigma_i$ were examined. One can see that the inaccuracy of the lateral trap position evaluation for characteristics with coefficients within $[\langle P_i\rangle\text{-}\sigma_i,\ \langle P_i\rangle+\sigma_i]$, which are the most wide-spreaded, does not exceed 5 nm. In the case of extremely strong impact of random dopants, when the $\Delta V_{\mathrm{th}}(V_{\mathrm{d}})$ shape strongly deviates from the average one (i.e. $[\langle P_i\rangle\text{-}3\sigma_i,\ \langle P_i\rangle+3\sigma_i]$), the error is not more than 10 nm, even if the trap is situated in the middle of the channel. This is still better than our knowledge about technological parameters of the devices and thus sufficient for the practical application of our method for the characterization of industrial MOSFETs.

VII. Results and Discussions

Application of the method to the experimental data (Fig. 1, $N_{\mathrm{D}}\approx6\times10^{17}\,\mathrm{cm}^{-3}$) allowed us to extract the positions of all 9 traps. Initially the TCAD simulations data have been used as a reference in our trap location method and the obtained results plotted in terms of the normalized probability density are given in Fig. 9(top). One can see that the traps can be located with a high accuracy inside narrow intervals. The width of these intervals is typically related to the impact of the random dopants, and thus for the traps situated near the middle of the channel the distributions are wider.

However, the entire procedure may be significantly simplified if the TCAD simulations could be replaced by the compact model, because the TCAD simulations require several weeks of cluster simulations and the compact model provides the results in several minutes. These results are shown in Fig. 9(bottom). The distributions look similar to the TCAD case and the difference in X_{T} values extracted for the same traps is typically less than 10 nm. Thus, we conclude that the application of our trap location technique using the reference data obtained with help of our compact model is quite appropriate and allows to perform a rather fast characterization of the border traps in MOSFET without essential loss in accuracy.

VIII. Conclusions

A new method to determine the lateral trap position in nanoscale MOSFETs is proposed. In contrast to other tech-

niques, we take random dopants into account as these have a dramatic impact on the potential distribution inside the device. Still, our technique is able to locate traps with a precision of several nanometers by exploiting the fact that the slope and curvature of the $\Delta V_{\text{th}}(V_{\text{d}})$ dependence of single traps is considerably less sensitive to the random dopants than to the lateral trap position. In addition, we derived a compact model which allows to calculate the reference data for the algorithm without running time-consuming TCAD simulations. The substitution of TCAD data by compact results leads to only a small loss in accuracy but improves the efficiency by several orders of magnitude.

IX. Acknowledgements

The authors are thankful for the support obtained from the Austrian Science Fund (FWF) project No. p23958 and the EC's FP7 project No. 261868 (MORDRED).

References

[1] T. Grasser, B. Kaczer, W. Gös, H. Reisinger, T. Aichinger, P. Hehenberger, P.-J. Wagner, J. Franco, M. Toledano-Luque, and M. Nelhiebel, "The Paradigm Shift in Understanding the Bias Temperature Instability: From Reaction-Diffusion to Switching Oxide Traps," *IEEE Trans Electron Dev.*, vol. 58, no. 11, pp. 3652–3666, 2011.

[2] P. Lenahan, "Atomic Scale Defects Involved in MOS Reliability Problems," *Microelectronic Engineering*, vol. 69, no. 2-4, 2003.

[3] S. Lee, H.-J. Cho, Y. Son, D. S. Lee, and H. Shin, "Trap location," in *IEDM Technical Digest – 2009*, 2009, pp. 763–766.

[4] A. Asenov, R. Balasubramaniam, A. R. Brown, and H. Davies, "Trap location," *IEEE Trans. Electron Dev.*, vol. 50, pp. 839–844, 2003.

[5] M. Toledano-Luque, B. Kaczer, T. Grasser, P. Roussel, J. Franco, and G. Groeseneken, "Toward a streamlined projection of small device bias temperature instability lifetime distributions," *J. Vac. Sci. Technol. B*, vol. 31, no. 1, pp. 01A114–1–01A114–4, 2013.

[6] M. Toledano-Luque, B. Kaczer, P. Roussel, M. Cho, T. Grasser, and G. Groeseneken, "Temperature dependence of the emission and capture times of SiON individual traps after positive bias temperature stress," *J. Vac. Sci. Technol. B*, vol. 29, no. 1, pp. 01AA04–1–01AA04–5, 2011.

[7] B. Kaczer, P. Roussel, T. Grasser, and G. Groeseneken, "Statistics of Multiple Trapped Charges in the Gate Oxide of Deeply Scaled MOSFET Devices-Application to NBTI," *IEEE Electron Dev. Lett.*, vol. 31, no. 5, pp. 411–413, 2010.

[8] T. Grasser, H. Reisinger, W. Goes, T. Aichinger, P. Hehenberger, P.-J. Wagner, M. Nelhiebel, J. Franco, and B. Kaczer, "Switching Oxide Traps as the Missing Link Between Negative Bias Temperature Instability and Random Telegraph Noise," in *Proc. International Electron Devices Meeting (IEDM)*, 2009.

[9] R. Dreesen, K. Croes, J. Manca, W. D. Ceunick, L. D. Schepper, A. Pergoot, and G. Groeseneken, "A new degradation model and lifetime extrapolation technique for lightly doped drain nMOSFETs under hot-carrier degradation," *Microel. Reliab.*, vol. 41, pp. 437–443, 2001.

[10] A. Lelis and T. Oldham, "Time Dependence of Switching Oxide Traps," *IEEE Transactions on Nuclear Science*, vol. 41, no. 6, pp. 1835–1842.

[11] A. Sarwar, M. Siddiqui, R. Siddiqui, and Q. Khosru, "Effects of interface traps and oxide traps on gate capacitance of MOS devices with ultrathin (EOT $\sim$ 1 nm) high-k stacked gate devices," *TENCON*, pp. 1–5, 2009.

[12] E. Hsieh, Y. Tsai, S. Chung, C. Tsai, R. Huang, and C. Tsai, "The Understanding of Multi-level RTN in Trigate MOSFETs Through the 2D Profiling of Traps and Its Impact on SRAM Performance: A New Failure Mechanism Found," in *IEDM Technical Digest – 2009*, 2012, pp. 454–457.

[13] T. Grasser, K. Rott, H. Reisinger, P.-J. Wagner, W. Gös, F. Schanovsky, M. Waltl, M. Toledano-Luque, and B. Kaczer, "Advanced Characterization of Oxide Traps: The Dynamic Time-Dependent Defect Spectroscopy," in *IRPS*, 2013, pp. 1–6.

[14] T. Grasser, H. Reisinger, P.-J. Wagner, and B. Kaczer, "Time-Dependent Defect Spectroscopy for Characterization of Border Traps in Metal-Oxide-Semiconductor Transistors," *Phys. Rev. B*, vol. 82, pp. 245 318–1–245 318–10, 2010.

[15] M. Waltl, P.-J. Wagner, H. Reisinger, K. Rott, and T. Grasser, "Advanced Data Analysis Algorithms for the Time-Dependent Defect Spectroscopy of NBTI," in *Proc. International Integrated Reliability Workshop (IIRW)*, 2012, pp. 74–79.

[16] M. Ancona, N. Saks, and D. McCarthy, "Lateral disrtribution of hot-carrier-induced" interface traps in MOSFET's," *IEEE Trans Electron Dev.*, vol. 35, no. 12, pp. 221–2228, 1988.

[17] T. Cochet *et al.*, in *ESSDERC*, 1999, pp. 680–683.

[18] C. Y. Wu and S. Y. Yuang, "Trap location," *Solid-State Electron*, vol. 27, pp. 651–658, 1984.

[19] Y. S. Jean and C. Y. Wu, "Trap location," *IEEE Trans. Electron Dev.*, vol. 44, pp. 441–447, 1997.

[20] Y. Illarionov, S. Tyaginov, M. Bina, and T. Grasser, "A method to determine the lateral trap position in ultra-scaled MOSFETs," in *SSDM*, 2013, pp. 278–279.

[21] G. Angelov and K. Asparuhova, "MOSFET Simulation Using Matlab Implementation of the EKV Model," in *ELECTRONICS'2006*, 2006, pp. 167–172.